ACS APPLIED ELECTRONIC MATERIALS

pubs.acs.org/acsaelm Article

Selective Purity Modulation of Semiconducting Single-Walled Carbon Nanotube Networks for High-Performance Thin-Film Transistors

Hayun Kim, Hyunuk Oh, Hyunjun Yoo, Kyungjune Cho, Takhee Lee, Seungjun Chung, Byeongmoon Lee,* and Yongtaek Hong*

Cite This: ACS Appl. Electron. Mater. 2023, 5, 2055−2064 Read Online

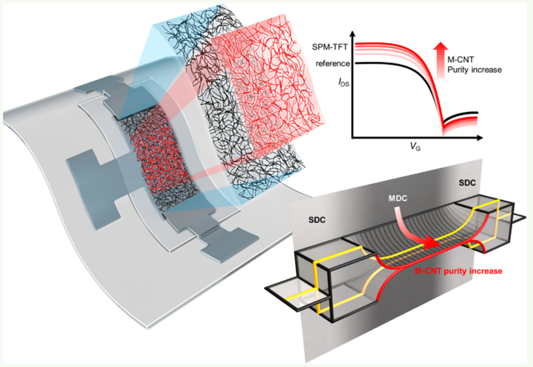

ABSTRACT: Single-walled carbon nanotube (SWCNT) random networks have become strong candidates for next-generation electronics due to their exceptional mechanical, electrical, and optical properties. However, metallic nanotubes in networks generally incur a trade-off between the charge carrier mobility and on/off ratio, limiting the performance of SWCNT-based devices. Therefore, various methods to increase the purity of semiconducting nanotubes in entire random networks have been reported, but this direction has faced other issues, such as nanotube shortening, higher cost, and higher energy. Here, we introduce SWCNT random network-based thin-film transistors (SWCNT TFTs) with a varying purity profile of semiconducting SWCNTs across the channel, exploiting the superior mobility of metallic SWCNTs by partially tuning the semiconducting SWCNT purity and developing a novel perspective on metallic nanotubes in semiconductor channels. Based on the high-precision drop-on-demand capability of inkjet printing and various concentrations of semiconducting SWCNT ink, we form selectively patterned channel regions with different semiconducting SWCNT purities. The metallic nanotube-dominant region drastically increases the carrier density with a minimized Schottky barrier, while high-purity semiconducting regions at the channel boundaries effectively block off-state leakage through carrier depletion. As a result, the SWCNT TFTs with selectively patterned metallic nanotube regions show superior carrier mobility (75.50 cm^2 V^{-1} s^{-1}) and channel width normalized on-current (34.33 nA μm^{-1}) without compromising the on/off ratio (1.62×10^7). To show the feasibility of our device in high-performance electronics, we demonstrate all-inkjet-printed flexible display driving circuits with two transistors that enable low-power, high-performance operation in display applications.

KEYWORDS: *single-walled carbon nanotube, thin-film transistor, channel purity engineering, energy band engineering, inkjet printing, percolation pathway*

■ INTRODUCTION

In recent years, single-walled carbon nanotube (SWCNT) networks have drawn significant interest in both industry and academia for their impressive mechanical, electrical, optical, and thermal properties.[1−5] In particular, their customized processability,[6−9] superior electrical charge carrier mobility,[10,11] and low Schottky barrier (SB) with metal electrodes[12−14] are the most favorable for transistors for next-generation electronics. However, metallic SWCNTs (M-CNTs) randomly distributed in as-grown SWCNT networks form leakage paths while boosting the carrier mobility, creating a strong and long-standing trade-off between the carrier mobility and on/off ratio.[15,16] In this regard, many efforts have been made to completely eliminate M-CNTs from channels via sorting methods such as density gradient ultracentrifugation,[17] gel chromatography,[18] DNA wrapping,[19] dielectrophoresis,[20] and conjugated polymer wrapping.[21] However, these methods generally require high energy and costs or cause other performance issues arising from nanowire shortening. Furthermore, homogeneous, isotropic random networks of even highly purified semiconducting SWCNTs (S-CNTs) still cannot enhance the performance due to the limited carrier density of S-CNTs themselves and junction-induced mobility degradation. To alleviate these issues, anisotropic or additional geometries have been employed in channel regions, such as network density profiles,[22] nanotube alignment,[23] and double-gate structures.[9] However, they are still uncompetitive

Received: December 9, 2022
Accepted: March 10, 2023
Published: March 22, 2023

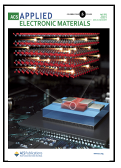

https://doi.org/10.1021/acsaelm.2c01685
ACS Appl. Electron. Mater. 2023, 5, 2055−2064

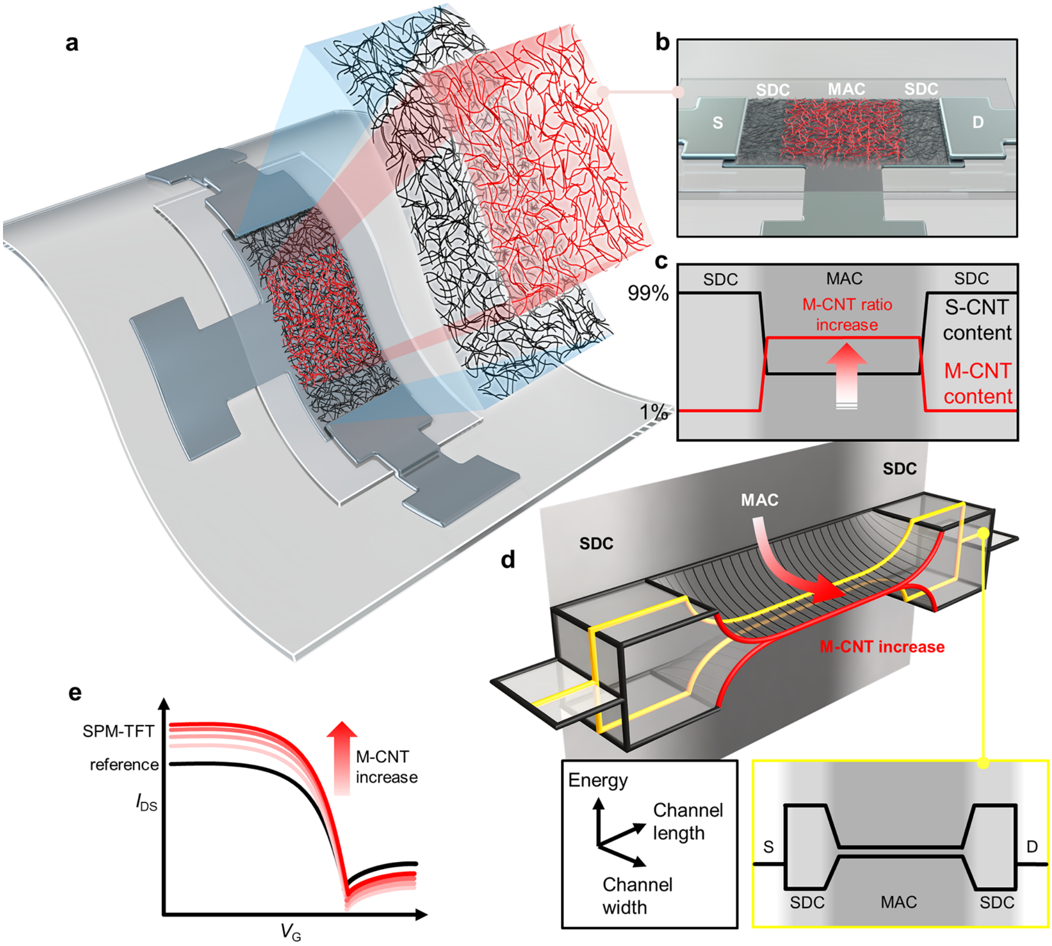

Figure 1. (a) Conceptual illustration of an all-inkjet-printed SPM-TFT on a flexible PEN substrate and (b) additionally printed M-CNT area in the SPM-TFT channel. (c) Gradation of the S-CNT and M-CNT purity along the channel direction and (d) energy band diagram of the SPM-TFT according to the M-CNT ratio in the MAC area. (e) Conceptual transfer curves showing the I_{on} increase and I_{off} decrease in the SPM-TFT according to the M-CNT ratio in the MAC area.

compared to industrial transistors in terms of both performance and fabrication complexity, limiting a window of performance engineering around the previous trade-off curve.

In this work, we report a universal, scalable, and highly customizable method for SWCNT thin-film transistors (TFTs) that offers a wide spectrum of performance engineering far deviated from the previous upper bound. Unlike previous approaches that exclude M-CNTs, we partially utilize the superior carrier mobility of M-CNTs in a random network by introducing a spatially varying purity profile of S-CNT across the channel. Specifically, we engineer the S-CNT purity of the channel center differentiating the M-CNT content of the area. At the source/drain (S/D) junction areas, S-CNT dominant channel (SDC) areas are formed. At the middle of the channel, an additional M-CNT is printed and forms an M-CNT added channel (MAC) area, where an excessive amount of M-CNTs significantly increases the carrier concentration by forming a percolation pathway.[24] Therefore, the MAC acts as a highly carrier-doped semiconductor with a narrow bandgap, facilitating hole transport and thereby resulting in higher on-current and carrier mobility. At the same time, the SDC areas at the channel boundaries act as depletion regions under reverse bias, efficiently blocking the off-state leakage current. Varying the S-CNT purity of the channel center allows us to continuously adjust the device performance of semiconducting purity modulated SWCNT TFTs (SPM-TFTs) such as on-current (I_{on}), off-current (I_{off}), and mobility by controlling the MAC fabrication parameters such as the purity and density of M-CNTs. As a result, the device with optimized MAC parameters achieves remarkably high hole mobility (75.50 cm^2 V^{-1} s^{-1}) and a channel width (W) normalized on-current (I_{on}/W) of 34.33 nA μm^{-1} while maintaining an extremely low channel width normalized off-current (I_{off}/W) of 2.09 fA μm^{-1} and consequently a high on/off ratio (1.62 × 10^7). With tailored performance modification of SPM-TFTs, we also demonstrate an all-inkjet-printed flexible display driving circuit with two TFTs with different channel S-CNT purity, which has a higher maximum on-current and fine switching performance, highlighting the feasibility of our approach in industrial applications.

RESULTS AND DISCUSSION

Concept and Morphology of the SPM-TFTs. Figure 1a and b illustrate the concept and structure of our SPM-TFTs. The channel region was first formed by uniformly printing highly purified S-CNT ink (99%). The channel center's CNT content is then adjusted by additionally printing CNT ink from 90% purity S-CNT ink (which stands for 10% M-CNT) to 70% M-CNT ink. Accordingly, the SDC regions with fixed high S-CNT purity were located at the boundaries of the

https://doi.org/10.1021/acsaelm.2c01685
ACS Appl. Electron. Mater. 2023, 5, 2055−2064

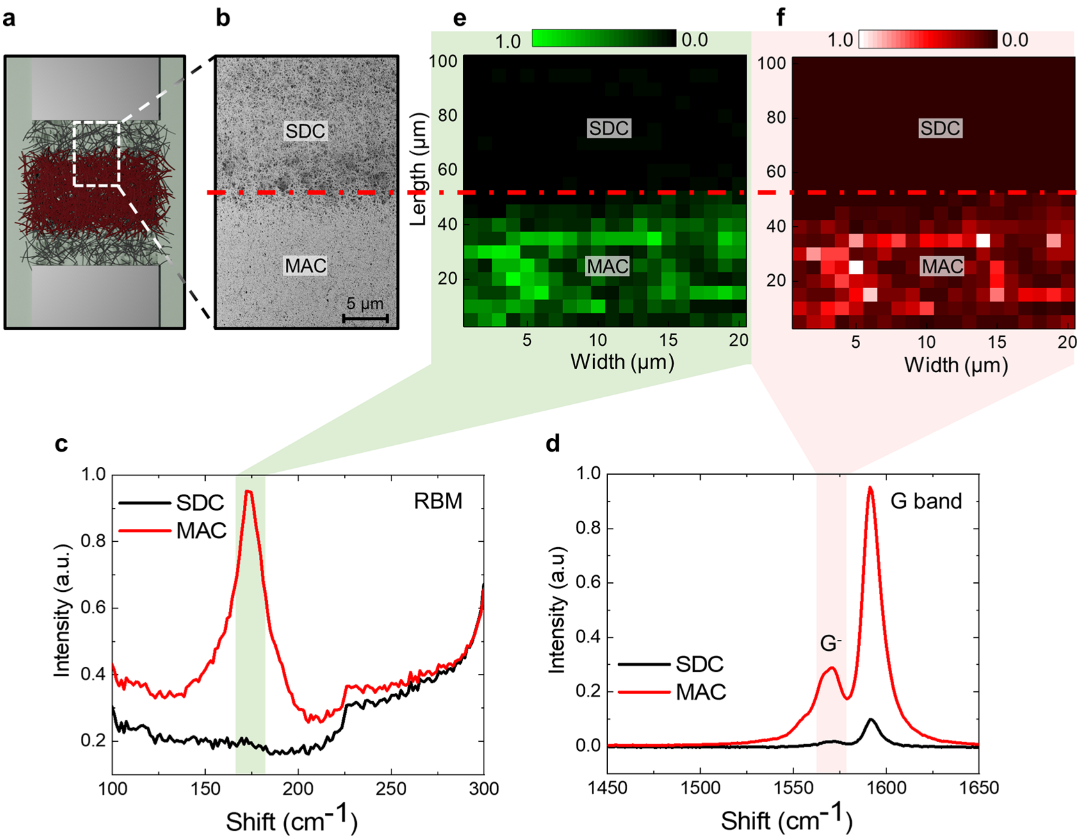

Figure 2. (a) Conceptual morphology of the selectively metalized channel and (b) SEM image of the channel area showing a boundary between MAC and SDC areas. Raman spectra taken with a 521 nm laser of the (c) RBM and (d) G band. Spatial map of the MAC and SDC areas obtained from integrated intensities (e) from 162 to 182 cm^{-1} and (f) from 1560 to 1580 cm^{-1}.

channel, containing a minimized amount of M-CNTs. The entire manufacturing process was based on inkjet printing, which allowed us to automatically and precisely define the geometries and levels of the SDC and MAC areas at a spatial resolution of 5 μm and a volume resolution of 10 picoliters. Figure 1c shows the S/M-CNT purity across the channel. While the SDC region maintains high-purity S-CNTs, the MAC region has a higher ratio of M-CNTs with lower S-CNT purity due to the additional printing of M-CNTs. The effect of the patterned M-CNT on the energy band structure is schematically illustrated in Figure 1d. As the S-CNT purity in the MAC decreases, increased M-CNTs form more percolation pathways, which gradually narrows the bandgap of the MAC.[25] For the SDC regions, the M-CNT depletion ensures a wide bandgap. In the on-state, a large number of carriers in the MAC increases carrier mobility and on-current. Furthermore, the anisotropic bandgap profile along the channel direction induces a large potential drop across the SDC areas and makes the SB between the S/D and the channel sharper and thinner, which facilitates hole tunneling and transport in the on-state (Figure 1e). In the off-state, the large bandgap of the SDC and carrier depletion due to the extremely low M-CNT content efficiently block electron injection and prevent an unwanted leakage current.

The morphology of the SDC and MAC was first characterized by scanning electron microscopy (SEM) (Figure 2a,b). The interface between the SDC and MAC in the SEM image clearly shows a stepwise increase in the CNT density. The calculated areal coverages of SWCNTs in the SDC and MAC areas are 52.2% and 71.2%, respectively, showing the distinct density difference between the two regions (Figure S1). Since M-CNTs and S-CNTs are indistinguishable in SEM images, we further carried out Raman spectroscopy to spatially characterize the metallicity in the channel. Compared to the SDC, the average spectra taken from the MAC show clear differences in the radial breathing mode (RBM) and G^- band. For the RBM (100−300 cm^{-1}), a specific peak at approximately 172 cm^{-1} is observed, indicating that CNTs of a specific diameter are concentrated in the MAC region.[20,26] In addition, the Raman spectra taken from the MAC region show a clear and broad G^- band (1560−1580 cm^{-1}), showing distinct chirality[27] and stronger electron−phonon coupling of M-CNTs (Figure 2c,d). The strong electron−phonon interaction in M-CNTs causes Kohn anomalies[28] in the phonon dispersion, and the low-frequency component of the G^- subband arises. Figure 2e and f show the spatial mapping of integrated intensities from 162 to 182 cm^{-1} and over the G^- band in the channel, which clearly shows the high portion of M-CNTs in the MAC.

Effect of the MAC Purity, Length, and Density. We characterized the transfer characteristics of the SPM-TFTs and compared them with those of uniform density and purity devices. To minimize the effect of fabrication parameters other than the density and purity profiles of the SWCNT channel, the devices were fabricated on a heavily doped p-type silicon wafer with a 200-nm-thick-grown dioxide layer. The channel width (W) and length (L) were fixed at 300 and 300 μm, respectively. We first compared three reference TFTs (RTFTs) with uniform purity S-CNTs, which contained 99%, 90%, or 30% S-CNTs (99-RTFT, 90-RTFT, 30-RTFT). The 99-RTFT

https://doi.org/10.1021/acsaelm.2c01685
ACS Appl. Electron. Mater. 2023, 5, 2055−2064

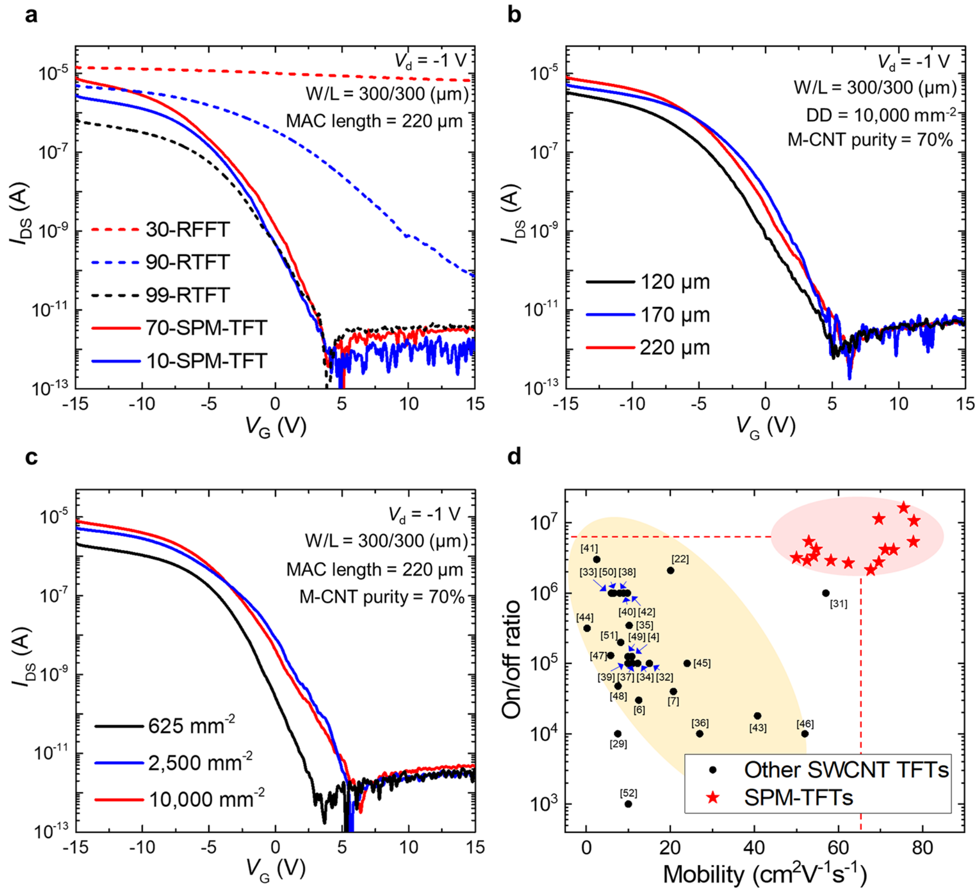

Figure 3. (a) Typical transfer characteristics of reference TFTs and SPM-TFTs. Transfer curves depending on the (b) MAC length (120, 170, and 220 μm) and (c) drop density in the MAC (625, 2500, and 10,000 mm^{-2}). (d) Relationship between the on/off ratio and mobility of SWCNT TFTs in previous studies and SPM-TFTs.

Table 1. Major Electrical Characteristics of the RTFTs, SPM-TFTs, and Ag-MAC-TFT

	99-RTFT	90-RTFT	30-RTFT	10-SPM-TFT	70-SPM-TFT (best/average)	Ag-MAC-TFT
mobility (cm^2·V^{-1}·s^{-1})	6.34	44.20	29.41	25.01	75.5/63.57 ± 10.30	27.9
I_{on} (μA)	0.65	7.69	11.00	2.12	10.30/7.39 ± 1.68	2.95
$\log_{10}(I_{on}/I_{off})$	5.43	4.90	0.50	6.27	7.21/6.62 ± 0.28	5.85
I_{off} (pA)	2.44	25.31	7.20 (μA)	1.20	0.63/2.02 ± 1.23	4.17
SS (mV/decade)	182.44	1856.70	46.28 (V/decade)	204.29	90.80/193.21 ± 0.14	198.68
V_{TH} (V)	1.30	15.00		1.55	2.8/2.21 ± 1.89	1.69

and 90-RTFT were made by printing 99% and 90% purity S-CNTs, respectively, and the 30-RTFT was fabricated by printing 70% purity M-CNTs over the entire channel area. Different ink compositions are identified by ultraviolet−visible (UV−vis) spectroscopy (Figure S2). In these uniform TFTs, as the purity of S-CNTs decreases, the rise in I_{off} is much greater than that in I_{on}, resulting in a reduced on/off ratio. Additionally, a severe shift of the threshold voltage (V_{TH}) around 2 V is observed in the case of a low S-CNT purity device. In the case of the 30-RTFT, the device almost loses its transistor characteristics due to the rapid rise in I_{off} (Figure 3a, Table 1).

However, the effect of M-CNTs is different in the case of the SPM-TFTs. For the SPM-TFTs, a fixed S-CNT purity of 99% was used to form the SDC areas, and two different M-CNT inks of 10% and 70% were additionally printed at MAC (10-SPM-TFT, 70-SPM-TFT). The 10-SPM-TFT shows low I_{off} (1.20 pA), which corresponds to an I_{off}/W of 3.99 fA μm^{-1} and excellent switching behavior, including low V_{TH} and subthreshold swing (SS). The device also exhibits good on-state characteristics in terms of I_{on} (2.12 μA), which corresponds to an I_{on}/W of 7.08 nA μm^{-1} and mobility of 25.01 cm^2 V^{-1} s^{-1}, which is 3.5 times higher than that of the 99-RTFT, achieving an on/off ratio of 1.86 × 10^6. The performance enhancement is even more pronounced in the case of the 70-SPM-TFT. The 70-SPM-TFT shows notable I_{on} (10.30 μA), which corresponds to an I_{on}/W of 34.33 nA μm^{-1} and fine mobility of 75.5 cm^2 V^{-1} s^{-1}, 16 and 12 times higher than those of the 99-RTFT while maintaining low I_{off} (I_{off} = 0.63 pA, I_{off}/W = 2.09 fA μm^{-1}) and great switching performance comparable to that of the 99-RTFT. That is, as the M-CNT concentration of the MAC increases in SPM-TFTs, I_{on} and mobility also increase without compromising the off-state properties. As a result, the SPM-TFT shows a surprising on/off ratio of 1.62 × 10^7.

The influence of the MAC length and density was further investigated by varying the printing area and the printing drop

https://doi.org/10.1021/acsaelm.2c01685
ACS Appl. Electron. Mater. 2023, 5, 2055−2064

density (DD), which is an inkjet-printer-controlled droplet number per 1 mm^2. First, to explore the change in the performance with the MAC length, devices with varying MAC lengths of 120, 170, and 220 μm were fabricated under a fixed total channel length of 300 μm (Figure 3b). As the MAC length increases, the I_{on} of the device gradually increases while maintaining a comparatively low I_{off}. In addition, we varied the DD of the M-CNT ink from 625 mm^{-2} to 10,000 mm^{-2} to investigate the influence of the M-CNT density under a fixed MAC length (220 μm). As shown in Figure 3c, the SPM-TFT fabricated under a DD of 10,000 mm^{-2} has the highest I_{on}. Namely, the performance enhancement is maximized as the MAC length and density increase. As a result, the optimized 70-SPM-TFT (n = 15, MAC length = 220 μm, DD = 10,000 mm^{-2}) shows the best performance (I_{on} = 7.39 ± 1.68 μA, mobility = 63.57 ± 10.30 cm^2 V^{-1} s^{-1}, I_{off} = 2.02 ± 1.23 pA, on/off ratio = 4.17 × $10^{6±0.28}$), with high reproducibility (Figure S3 and Table 1). These values correspond to a more than 11 times higher I_{on}, a 10 times higher mobility, and a 70 times higher on/off ratio compared to the 99-RTFT. Figure 3d compares the mobilities and on/off ratios of SWCNT TFTs in the literature.[4,6,7,22,29−52] Previously reported TFTs based on SWCNT random networks exhibit a strong negative correlation between the mobility and on/off ratio. In contrast, our SPM-TFTs are located completely away from the trade-off trend area, simultaneously exhibiting the highest mobility and on/off ratio.

In order to investigate the unique characteristics of SPM-TFTs, two transistors connected in series with the connecting electrode length the same as the MAC length of 220 μm were fabricated in order to distinguish the difference between SPM-TFT and serially connected two short-channel TFT. Since the fabricated device has the same structure and fabrication process as the SPM-TFT except that Ag was printed for its MAC, it is referred to as a Ag-MAC-TFT. Although the Ag-MAC-TFT shows enhanced performance (I_{on} = 2.95 ± 0.54 μA, mobility = 27.9 ± 6.0 cm^2 V^{-1} s^{-1}) compared to the RTFTs, the increase is much lower than that in the SPM-TFT (Figures S3a,b, Table 1). The limited performance of Ag-MAC-TFT will be further discussed in the mechanism part. Furthermore, a single transistor with a short channel length (80 μm) that is the same as the sum of the SDC lengths of SPM-TFT was compared to the SPM-TFT (Figures S3c). In this case, the SPM-TFT clearly showed a higher on/off ratio of 3.98 × 10^6 compared to 1.70 × 10^6 of the short-channel transistor. The higher performance of the SPM-TFT is attributed to the low I_{off} without any side effects. Furthermore, a V_{TH} shift of more than 2 V was observed in single-transistor devices, which is a chronic problem of SWCNT TFTs caused by a decrease in percolation threshold as the channel is shortened. The I_{off} and V_{TH} shift retention performance of SPM-TFT is due to additional Schottky barriers existing between SDC and MAC inside the channel suppressing the carrier transporting under the off-state.

Transport Mechanism and Energy Band Profiles of the SPM-TFTs. We have demonstrated that the SPM-TFTs simultaneously show extremely high I_{on} and low I_{off}. These unique characteristics can be explained by the transport mechanism[53] of S/M-CNTs and the energy band profile modulated by selectively patterned M-CNTs in the channel. In the SWCNT-based channel, the current induced by hole carrier hopping is strongly facilitated by charged M-CNTs since M-CNTs work as a shortcut for carriers to move along the channel direction. Figure 4a and b compare the SWCNT random networks without and with MAC. The 99-RTFT

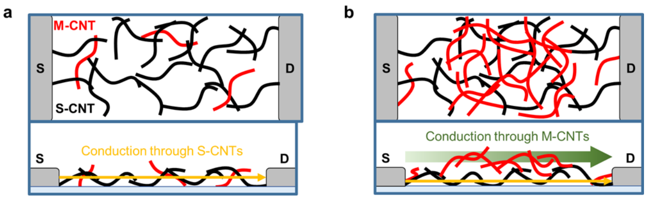

Figure 4. Conceptual illustration of S-CNT and M-CNT dispersions in the channels of the (a) 99-RTFT and (b) 70-SPM-TFT.

contains a minimized amount of M-CNTs, where the carrier mobility is limited due to the lack of connected paths of M-CNTs (Figure 4a). In other words, the long distance between M-CNTs makes the carrier hopping from one M-CNT to another difficult. In the case of the SPM-TFT, the MAC contains an excessive amount of M-CNTs which is higher than the percolation threshold, thus forming spanning clusters (Figure 4b). These highly conductive paths promote carrier mobility and I_{on} in the on-state. Additionally, in the off-state, the SDC becomes a carrier depletion region that effectively suppresses the leakage current. Namely, the MAC improves I_{on}, while the SDC maintains a low I_{off}.

To further explore the working principle of SPM-TFT in more detail, a conceptual equivalent energy band diagram model assuming M-CNT as a narrow bandgap material is deliberated in Figure S3a−c. Figure S3a shows the energy band diagram of the RTFTs made of high-purity S-CNTs. The wide bandgap of S-CNTs forms a high and thick SB, which blocks hole tunneling from the source to the channel. In contrast, for the equivalent model of the SPM-TFTs, the SB between the S/D and channel is sharper and thinner due to the large potential drop across the SDC in the on-state, which results from the bandgap difference between the SDC and MAC assuming M-CNT as a narrow bandgap material (Figure S3b).[12,15] This sharp, thin SB facilitates hole tunneling from the source to the channel, inducing high I_{on}. Once the carriers flow into the MAC, they are efficiently transported through the highly conductive M-CNT network. The mechanism is also verified through the experimental results, where the SPM-TFTs with a shorter SDC and a denser MAC show higher I_{on}. In the off-state, two leakage mechanisms, i.e., thermionic hole transport at intermediate V_G and electron tunneling at high V_G, exist. For the RTFTs, as the concentration of M-CNTs increases, the SB height decreases, facilitating carrier transport and resulting in high I_{off}. Accordingly, the 99-RTFT exhibits the highest SB and consequently the lowest leakage current. The SPM-TFT has the same advantage as the 99-RTFT since it also contains two SDC regions at the S/D junction (Figure S3b). These SDCs form a high potential barrier that efficiently blocks hole tunneling from the source at intermediate V_G and electron injection into the drain at high V_G.

Another reason that the SPM-TFTs can achieve maximized carrier mobility is that the M-CNTs inside the MAC form a minimized SB[57] with the S-CNTs (half of the bandgap of S-CNTs)[15] because of their identical Fermi levels. In contrast, other metals would form a heterojunction with S-CNTs with a higher SB,[54] limiting carrier transport between the metallic and semiconducting area. To investigate the effect of the SB height, we compared the performance of Ag-MAC-TFT and SPM-TFT. The Ag metal was selected due to its printing

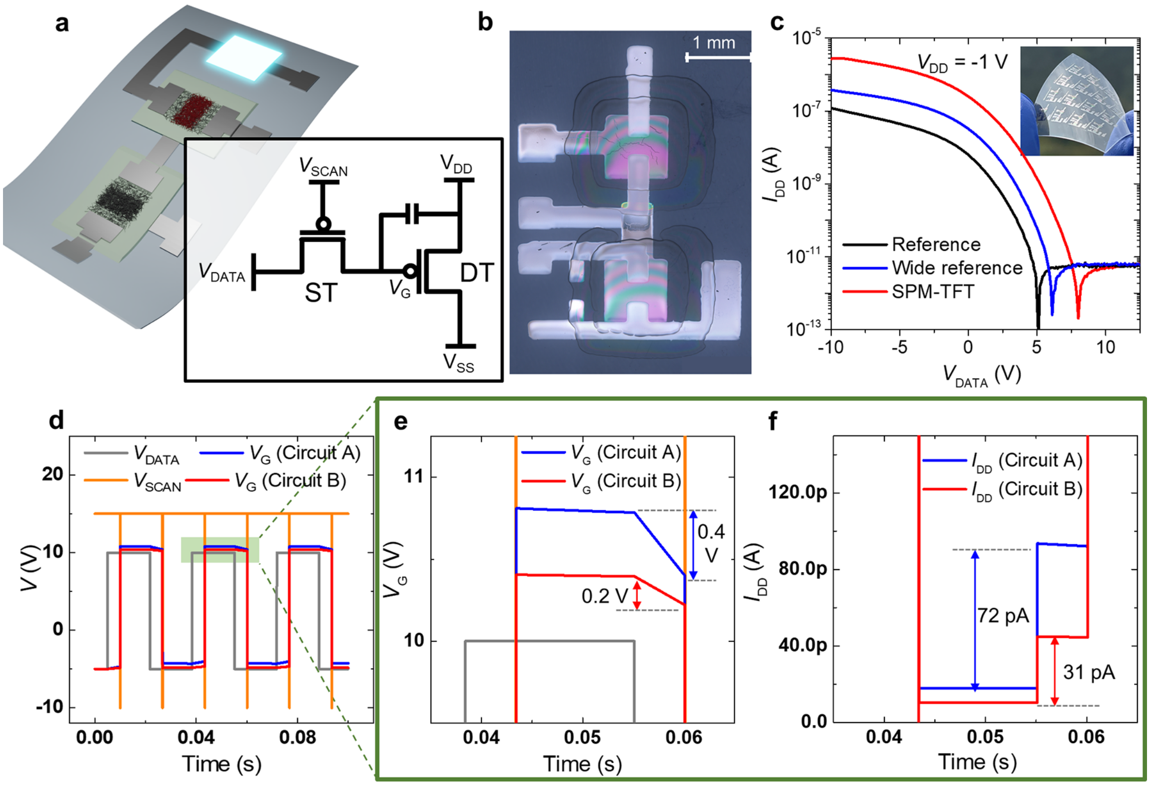

Figure 5. (a) Conceptual illustration and schematic of the display driving circuit and (b) optical image of the fabricated driving circuit on a flexible PEN substrate. (c) $I_{DD}-V_{DATA}$ characteristics of the reference, wide reference, and SPM-TFT as a DT and optical image of the fabricated driving circuit array. For a 60 Hz active matrix white−black display, simulation results of circuits A (using RTFT) and B (using SPM-TFT) in terms of the (d) voltages, (e) voltage change within a single frame, and (f) current fluctuation within a single frame at the V_G node.

processability. Although the Ag-MAC-TFT shows enhanced I_{on} and mobility performance compared to the RTFTs, the increase is much lower than that in the SPM-TFT (Figure S4, Table 1). The limited performance of the Ag-MAC-TFT can be attributed to the high SB formed between the S-CNT-based SDC and Ag-MAC that arises from the difference between the work function of Ag (∼4.2 eV) and the Fermi energy of CNTs (∼4.5 eV)[55,56] (Figure S3c). As a result, the high and thick SB disturbs the carrier transport at the interface between the SDC and Ag-MAC, leading to lower I_{on} and mobility.

We also extracted the channel sheet resistance (R_s) and contact resistance between the S/D and channel (R_c) of the SPM-TFT and Ag-MAC-TFT with the Y-method[58,59] to verify the SB height difference (Figure S5). Unlike R_c, which is similar for SPM-TFT and Ag-MAC-TFT, the R_s of the SPM-TFT is approximately seven times smaller than that of the Ag-MAC-TFT, which can be attributed to the SB height difference between S-CNT/M-CNT and S-CNT/Ag.

Simulation for All-Inkjet-Printed Display Driving Circuits Using SPM-TFTs. To show the feasibility of our SPM-TFTs in high-performance electronics, we demonstrated all-inkjet-printed display driving circuits without storage capacitors using SPM-TFTs on flexible substrates. All deposition processes of electrodes, dielectrics, and channel layers were conducted by inkjet printing on a flexible polyethylene naphthalate (PEN) substrate. Appropriate performance tuning of SPM-TFTs was achieved for meeting different requirements of driving transistors (DT) and scanning transistors (ST) without additional fabrication processes or size expansion, whose advantages were properly verified by experiments and simulation. Figure 5a and b show a schematic and an optical image of the fabricated driving circuit. Typically, the display driving circuit consists of an array of two transistors and a single capacitor as a group (Figure 5a). When the ST is turned on, V_{DATA} is delivered to the V_G node of the DT. Then, the voltage difference between V_{DD} and V_G is stored in a capacitor, turning on the LED at the desired brightness regardless of the V_{DATA}.

To verify the superiority of the driving circuits using our SPM-TFTs, three circuits comprising different DTs of a 99-RTFT (W/L = 300/300 μm), a 99-RTFT (W/L = 600/300 μm), and an SPM-TFT (W/L = 300/300 μm) were fabricated, which were referred to as the reference circuit, wide-reference circuit, and SPM-TFT circuit, respectively. The same 99-RTFT (W/L = 300/300 μm) was used for an ST. Figure 5c compares the $I_{DD}-V_{DATA}$ characteristics of the three different driving circuits at a V_{DD} of 1.1 V (Figure S6). Although the wide-reference circuit shows an increased on-state I_{DD} due to the doubled width of the DT compared to the reference circuit, it inevitably compromises the spatial resolution in display applications. In contrast, the SPM-TFT circuit exhibits the highest I_{DD} (2.67 μA), 22 times higher than that of the reference circuit, without sacrificing other electrical properties or requiring extra space. Accordingly, the SPM-TFT circuit can maximize the luminance of the white color displayed by the OLED with a low-power operation.

Furthermore, since it was difficult to fabricate the storage capacitor through the solution process, we simulated a 60 Hz active-matrix white−black display with data gathered from the ST, DT, and virtual storage capacitor to verify the effect of the improved performance of the driving circuits on the display operation when using SPM-TFTs. We compared two circuits

https://doi.org/10.1021/acsaelm.2c01685
ACS Appl. Electron. Mater. 2023, 5, 2055−2064

based on RTFTs and SPM-TFTs. Circuit A comprised a 99-RTFT (W/L = 300 μm/300 μm) for an ST and a 99-RTFT (W/L = 600 μm/300 μm) for a DT. In circuit B, a 10-SPM-TFT (W/L = 300 μm/300 μm) was used for an ST requiring low I_{off} and a 70-SPM-TFT (W/L = 300 μm/300 μm) was used for a DT requiring high I_{on} (Table 2). The transfer curves of the unit TFTs for the simulation were fitted based on the measured data (Figure S7). Figure 5d−f presents the simulation results of turning the display on (V_{DATA} = −5 V) and off (V_{DATA} = 10 V) repeatedly showing V_G over time according to the output current change of the ST. The simulation assumed a display driving circuit with 1080 lines, turning on and off the LED at a frequency of 60 Hz for one of the lines. Accordingly, the V_{DD} value was fixed at 10 V and the V_{SCAN} value repeated the operation of turning the ST on (−10 V) for 0.0155 ms and off (5 V) for 16.68 ms (simulation details in Figure S7). In the case of the black display as enlarged in Figure 5e, as V_{DATA} abruptly drops from 10 V to −5 V in the middle of a single frame, a V_G drop occurs due to the large V_{DS} of the ST. Circuit A with a higher I_{off} of the ST suffers from a larger voltage drop of close to 0.4 V than that of circuit B (0.2 V), and this voltage drop leads to a sharp I_{DD} upswing of 72 pA (Figure 5f), which can cause a luminance change in a single black frame, i.e., a flicker, which is a critical issue in practical display devices. In contrast, circuit B with a lower I_{off} of the SPM-TFT for the ST suffers less voltage drop and efficiently suppresses the I_{DD} increase to 31 pA. Also, circuit B shows a much higher I_{DD} with a smaller width of the channel than reference circuit A (Figure S8). The simulation results reveal that the display driving circuit with SPM-TFTs can maximize the luminance and minimize the flicker issue, highlighting that our approach can significantly improve the performance of practical display applications.

Table 2. Simulation Conditions of Circuits A and B for the ST and DT of the Display Driving Circuit

	circuit A	circuit B
ST	99-RTFT (W/L = 300 μm/300 μm)	10-SPM-TFT (W/L = 300 μm/300 μm)
DT	99-RTFT (W/L = 600 μm/300 μm)	70-SPM-TFT (W/L = 300 μm/300 μm)

■ CONCLUSION

We have demonstrated all-inkjet-printed SWCNT TFTs with continuous performance tunability which shows high I_{on}/W (34.33 nA μm^{-1}), high mobility (75.5 cm^2 V^{-1} s^{-1}), and low I_{off}/W (2.09 fA μm^{-1}) simultaneously at optimized conditions. They have a spatially distinguished S-CNT purity profile across the channel, where the SDC areas contain highly purified S-CNTs at the channel boundaries and the MAC area contains lower purity S-CNTs with a larger M-CNT ratio in the middle of the channel. The M-CNTs in the MAC form highly conductive percolation networks with a minimized SB, facilitating hole transport in the on-state. Furthermore, the MAC leads to sharp and thin SBs at the channel boundaries, facilitating hole tunneling from the S/D to the channel. In contrast, the high and thick SB formed by the SDC areas, which act as depletion regions, efficiently block hole tunneling and electron injection in the off-state. Compared to the literature, our method offers high tunability in the performance of SWCNT TFTs with a simple process, consequently breaking the conventional negative trade-off between the mobility and on/off ratio. Based on the SPM-TFTs, we successfully demonstrated all-inkjet-printed flexible display driving circuits on a flexible PEN substrate. The channel S-CNT purity profiles of the DT and ST were adequately engineered according to the required transfer characteristics. The experimental and simulation results reveal that our SPM-TFTs can significantly contribute to higher maximum luminance, higher contrast ratio, and lower power consumption in display applications.

Although the electrical performance has improved dramatically through the SPM-TFT structure, there is a limit that it has a relatively long channel length of 300 μm compared to commercialized transistors. But when incorporated with higher resolution printing technologies such as electrohydrodynamic printing, the SPM-TFTs with a shorter channel length could be realized, which can further push up on-state performances without compromising off-state stability. We believe that our study offers a new blueprint for modulating the properties of SWCNT channels and leads SWCNT TFTs toward commercial use in the field of high-performance electronics.

■ EXPERIMENTAL SECTION

Materials for the SPM-TFT. Isopropyl alcohol (IPA, Daejung Chemicals & Metals Co.) and acetone (Daejung Chemicals & Metals Co.) were sequentially used without any purification for cleaning the substrate. Silver ink (JET 004T, Kunshan Hisense Electronics Corp.) was printed to form source, drain, and gate electrodes. Aqueous poly-L-lysine (PLL) solution (0.1% (w/v) in H_2O, Sigma−Aldrich Corp.) was utilized to amine-functionalize the substrate surface. Semiconducting single-walled CNT solutions of 90%, 95%, and 99% purity (IsoNanotube-S, Nanointegris Corp.) and metallic single-walled CNT ink of 70% purity (IsoNanotube-M, Nanointegris Corp.) were used to form the channels of the TFTs. All CNTs have a diameter range of 1.2−1.7 nm, mean diameter of 1.4 nm, and mean length of ∼0.5 μm for IsoNanotube-M and ∼1 μm for IsoNanotube-S inks according to the provided technical data sheet.

Fabrication of SPM-TFTs. Heavily doped p-type silicon with a 200-nm-thick thermally grown silicon dioxide layer was used as a substrate for the devices. A piezoelectric inkjet printer (DMP-2831, Fujifilm Dimatix Corp.) was used to print every layer of the devices. The silicon substrate was sequentially bath ultrasonicated in acetone and IPA for 5 min each. Before printing, the substrate underwent UV ozone treatment for 5 min to form hydroxyl groups (−OH) on the silicon dioxide layer. Then, an amine-terminated surface was formed by drop casting a PLL solution on the surface for 5 min and rinsing the substrate with deionized (DI) water for 1 min to remove the remaining solution except for the PLL bound to the hydroxyl groups. The SWCNT ink was inkjet-printed to form an SWCNT random network on the oxide layer, followed by DI rinsing of 30 s to remove weakly bonded SWCNTs and residual surfactants. The process of printing and rinsing was repeated until the desired network density was achieved. S-CNT ink of 90% and 99% purity and 70% purity M-CNT ink were printed three times (DD = 625 mm^{-2}) to fabricate the different types of reference uniform purity TFTs. To fabricate the SPM-TFTs, 99% purity S-CNT ink was first printed (DD = 625 mm^{-2}) and rinsed three times, and 70% purity M-CNT ink (DD = 10,000 mm^{-2}) was additionally printed on a middle area of the channel and the S/D contact regions. M-CNT printing also involved the same printing and rinsing process and was conducted three times with a reduced rinsing time of 10 s. After printing the SWCNT layer, the substrate was annealed at 110 °C for 30 min on a hot plate to remove residual water molecules on the surface. After annealing, silver ink was inkjet-printed (DD = 816 mm^{-2}) at the desired position and annealed at 120 °C for 30 min on a hot plate to form S/D electrodes.

Fabrication of Ag-MAC-TFTs. The cleaning and surface treatment processes were the same as those for SPM-TFTs. In the

https://doi.org/10.1021/acsaelm.2c01685
ACS Appl. Electron. Mater. 2023, 5, 2055−2064

case of the Ag-MAC-TFT, which is two transistors connected in series with the connecting electrode length the same as the MAC length of 220 μm, 99% purity S-CNT ink was first printed (DD = 625 mm^{-2}), rinsed three times, and annealed under the same conditions as for SPM-TFTs. Then, silver ink was inkjet-printed (DD = 816 mm^{-2}) on the middle region of the channel in addition to at the S/D electrode positions and annealed at 120 °C for 30 min on a hot plate.

Materials for the All-Inkjet-Printed Flexible Driving Circuit. IPA (Daejung Chemicals & Metals Co.) and acetone (Daejung Chemicals & Metals Co.) were sequentially used without any purification for cleaning the substrate. Silver ink (JET 004T, Kunshan Hisense Electronics Corp.) was printed to form source, drain, and gate electrodes. For the dielectric layer, a polyvinylpyrrolidone (PVP) solution made of 10 wt % PVP powder (average molecular weight M_n ~ 25,000 g mol^{-1}, Sigma−Aldrich Corp.) and 2 wt % poly(melamine-*co*-formaldehyde) (M_n ~ 432 g mol^{-1}, Sigma−Aldrich Corp.) dissolved in propylene glycol methyl ether acetate (≥99.5%, Sigma−Aldrich Corp.) was used. Poly(melamine-*co*-formaldehyde) was added as a cross-linking agent to increase the capacitance and reduce hysteresis. Aqueous PLL solution (0.1% (w/v) in H_2O, Sigma−Aldrich Corp.) was utilized to amine-functionalize the substrate surface. Semiconducting single-walled CNT solutions of 90%, 95%, and 99% purity (IsoNanotube-S, Nanointegris Corp.) and metallic single-walled CNT ink of 70% purity (IsoNanotube-M, Nanointegris Corp.) were used to form the channels of the TFTs.

Fabrication of the All-Inkjet-Printed Flexible Driving Circuit. The driving circuit was fabricated on a 125-μm-thick PEN substrate. The PEN substrate was sequentially cleaned with acetone and IPA for 5 min each in an ultrasonic bath. After cleaning, the substrate was soft-baked in an oven for 1 h. Silver ink was first printed (DD = 816 mm^{-2}) on the cleaned substrate and annealed at 120 °C for 30 min on a hot plate to form a gate electrode. Next, a dielectric layer was formed by printing two layers of PVP solution (DD = 2500 mm^{-2}). The substrate was sequentially annealed on a hot plate after printing each layer at 100 °C for 30 min and 200 °C for 20 min to enhance the cross-linking of PVP. The channel, S/D electrodes, and circuit electrodes were inkjet-printed in turn with the same method as that for SPM-TFTs.

Characterization and Simulation. The electrical properties of the TFTs were measured by a semiconductor parameter analyzer (4145B, Agilent Technologies) at room temperature in a dark box and air atmosphere. SEM (S-4800, Hitachi, and Sigma 300, ZEISS) was used to obtain surface images of the SWCNT channel network. Raman spectroscopy was conducted with an XperRam 200 instrument (Nanobase, Inc.) with a 40× objective lens and a laser excitation wavelength of 532 nm under ambient conditions at room temperature to analyze the metallicity of SWCNTs across the channel. A simulation program with integrated circuit emphasis (SmartSpice, Silvaco) was used to model and simulate the performance of the display driving circuit with two transistors and one capacitor.

Mobility Extraction. Mobility at the linear region is extracted from eq 1.

$$I_{DS} = \frac{W}{2L}\mu C_{ox}[2(V_{GS} - V_{TH})V_{DS} - V_{DS}^2] \tag{1}$$

In our study, channel width (W) and length (L) are fixed parameters since they are defined with the inkjet-printing process. The capacitance of the dielectric layer (C_{ox}) and V_{DS} are also fixed parameters of 17 nF/cm^2 and −1 V since every transistor except for the display driving circuit uses a SiO_2 dielectric and uniform V_{DS}. V_{TH} is calculated with the gm, max method.

ASSOCIATED CONTENT

Supporting Information

The Supporting Information is available free of charge at https://pubs.acs.org/doi/10.1021/acsaelm.2c01685.

Detailed SEM images of the printed SWCNTs in the MAC and SAC areas; optical absorbance analysis of the S-CNT and M-CNT inks used to fabricate the SPM-TFTs; transfer curves of SPM-TFT, Ag-MAC-TFT, and short-channel single TFT; contact resistance and channel resistance of SPM-TFTs and the Ag-MAC-TFT; $I_{DD}-V_{DATA}$ curves of the TFTs used in display driving circuits; measured and accordingly fitted transfer curves of the TFTs used in the simulation and circuit schematic with simulated voltage condition at 60 Hz white−black display; I_{DD} of circuits A and B according to time in the condition of 60 Hz white−black display (PDF)

AUTHOR INFORMATION

Corresponding Authors

Byeongmoon Lee − *Department of Electrical and Computer Engineering, Inter-University Semiconductor Research Center (ISDC), Seoul National University, Seoul 08826, Korea; Soft Hybrid Materials Research Center, Korea Institute of Science and Technology, Seoul 02792, Korea;* orcid.org/0000-0001-9306-2435; Email: hardrist@kist.re.kr

Yongtaek Hong − *Department of Electrical and Computer Engineering, Inter-University Semiconductor Research Center (ISDC), Seoul National University, Seoul 08826, Korea;* orcid.org/0000-0001-9399-5948; Email: yongtaek@snu.ac.kr

Authors

Hayun Kim − *Department of Electrical and Computer Engineering, Inter-University Semiconductor Research Center (ISDC), Seoul National University, Seoul 08826, Korea;* orcid.org/0000-0001-7914-2543

Hyunuk Oh − *Department of Electrical and Computer Engineering, Inter-University Semiconductor Research Center (ISDC), Seoul National University, Seoul 08826, Korea;* orcid.org/0000-0002-1903-1064

Hyunjun Yoo − *Department of Electrical and Computer Engineering, Inter-University Semiconductor Research Center (ISDC), Seoul National University, Seoul 08826, Korea;* orcid.org/0000-0003-1030-5628

Kyungjune Cho − *Soft Hybrid Materials Research Center, Korea Institute of Science and Technology, Seoul 02792, Korea*

Takhee Lee − *Department of Physics and Astronomy, Seoul National University, Seoul 08826, Korea;* orcid.org/0000-0001-5988-5219

Seungjun Chung − *Soft Hybrid Materials Research Center, Korea Institute of Science and Technology, Seoul 02792, Korea;* orcid.org/0000-0002-4867-4149

Complete contact information is available at: https://pubs.acs.org/10.1021/acsaelm.2c01685

Author Contributions

H.K. and H.O. contributed equally to this work.

Notes

The authors declare no competing financial interest.

ACKNOWLEDGMENTS

This research was supported by National R&D Program through the National Research Foundation of Korea (NRF) funded by Ministry of Science and ICT (2020M3D1A2101801).

■ REFERENCES

(1) Wang, B. W.; Jiang, S.; Zhu, Q. B.; Sun, Y.; Luan, J.; Hou, P. X.; Qiu, S.; Li, Q. W.; Liu, C.; Sun, D. M. Continuous Fabrication of Meter-Scale Single-Wall Carbon Nanotube Films and their Use in Flexible and Transparent Integrated Circuits. *Adv. Mater.* **2018**, *30* (32), 1802057.

(2) Chen, Y. Y.; Sun, Y.; Zhu, Q. B.; Wang, B. W.; Yan, X.; Qiu, S.; Li, Q. W.; Hou, P. X.; Liu, C.; Sun, D. M. High-Throughput Fabrication of Flexible and Transparent All-Carbon Nanotube Electronics. *Adv. Sci.* **2018**, *5* (5), 1700965.

(3) Wang, W.; Wang, S.; Rastak, R.; Ochiai, Y.; Niu, S.; Jiang, Y.; Arunachala, P. K.; Zheng, Y.; Xu, J.; Matsuhisa, N.; et al. Strain-insensitive intrinsically stretchable transistors and circuits. *Nat. Electron.* **2021**, *4* (2), 143−150.

(4) Li, X.; Ren, Y.; Wang, X.; Shao, S.; Li, H.; Wu, L.; Liu, X.; Zhao, J. A Universal Method for High-Efficiency Immobilization of Semiconducting Carbon Nanotubes toward Fully Printed Paper-Based Electronics. *Adv. Electron. Mater.* **2021**, *7* (3), 2001025.

(5) Williams, N. X.; Bullard, G.; Brooke, N.; Therien, M. J.; Franklin, A. D. Printable and recyclable carbon electronics using crystalline nanocellulose dielectrics. *Nat. Electron.* **2021**, *4* (4), 261−268.

(6) Lu, S.; Zheng, J.; Cardenas, J. A.; Williams, N. X.; Lin, Y.-C.; Franklin, A. D. Uniform and stable aerosol jet printing of carbon nanotube thin-film transistors by ink temperature control. *ACS Appl. Mater. Interfaces* **2020**, *12* (38), 43083−43089.

(7) Kim, H.; Seo, J.; Seong, N.; Lee, S.; Lee, S.; Kim, T.; Hong, Y. Multidipping Technique for Fabrication Time Reduction and Performance Improvement of Solution-Processed Single-Walled Carbon Nanotube Thin-Film Transistors. *Adv. Eng. Mater.* **2020**, *22* (8), 1901413.

(8) Kim, B.; Jang, S.; Prabhumirashi, P. L.; Geier, M. L.; Hersam, M. C.; Dodabalapur, A. Low voltage, high performance inkjet printed carbon nanotube transistors with solution processed ZrO2 gate insulator. *Appl. Phys. Lett.* **2013**, *103* (8), 082119.

(9) Yoo, H.; Ha, J.; Kim, H.; Seo, J.; Lee, S.-Y.; Hong, Y. Tunable stability of all-inkjet-printed double-gate carbon nanotube thin film transistors. *IEEE Electron Device Lett.* **2020**, *41* (6), 860−863.

(10) Snow, E.; Campbell, P.; Ancona, M.; Novak, J. High-mobility carbon-nanotube thin-film transistors on a polymeric substrate. *Appl. Phys. Lett.* **2005**, *86* (3), 033105.

(11) Li, F.; Wang, H.; Kufer, D.; Liang, L.; Yu, W.; Alarousu, E.; Ma, C.; Li, Y.; Liu, Z.; Liu, C.; et al. Ultrahigh Carrier Mobility Achieved in Photoresponsive Hybrid Perovskite Films via Coupling with Single-Walled Carbon Nanotubes. *Adv. Mater.* **2017**, *29* (16), 1602432.

(12) Svensson, J.; Campbell, E. E. Schottky barriers in carbon nanotube-metal contacts. *J. Appl. Phys.* **2011**, *110* (11), 16.

(13) Javey, A.; Guo, J.; Wang, Q.; Lundstrom, M.; Dai, H. Ballistic carbon nanotube field-effect transistors. *Nature* **2003**, *424* (6949), 654−657.

(14) Nosho, Y.; Ohno, Y.; Kishimoto, S.; Mizutani, T. Relation between conduction property and work function of contact metal in carbon nanotube field-effect transistors. *Nanotechnology* **2006**, *17* (14), 3412.

(15) Snow, E.; Novak, J.; Campbell, P.; Park, D. Random networks of carbon nanotubes as an electronic material. *Appl. Phys. Lett.* **2003**, *82* (13), 2145−2147.

(16) Sun, D.-m.; Timmermans, M. Y.; Tian, Y.; Nasibulin, A. G.; Kauppinen, E. I.; Kishimoto, S.; Mizutani, T.; Ohno, Y. Flexible high-performance carbon nanotube integrated circuits. *Nat. Nanotechnol.* **2011**, *6* (3), 156−161.

(17) Arnold, M. S.; Green, A. A.; Hulvat, J. F.; Stupp, S. I.; Hersam, M. C. Sorting carbon nanotubes by electronic structure using density differentiation. *Nat. Nanotechnol.* **2006**, *1* (1), 60−65.

(18) Liu, H.; Nishide, D.; Tanaka, T.; Kataura, H. Large-scale single-chirality separation of single-wall carbon nanotubes by simple gel chromatography. *Nat. Commun.* **2011**, *2* (1), 1−8.

(19) Tu, X.; Manohar, S.; Jagota, A.; Zheng, M. DNA sequence motifs for structure-specific recognition and separation of carbon nanotubes. *Nature* **2009**, *460* (7252), 250−253.

(20) Krupke, R.; Hennrich, F.; Lohneysen, H. V.; Kappes, M. M. Separation of metallic from semiconducting single-walled carbon nanotubes. *Science* **2003**, *301* (5631), 344−347.

(21) Wang, H.; Bao, Z. Conjugated polymer sorting of semi-conducting carbon nanotubes and their electronic applications. *Nano Today* **2015**, *10* (6), 737−758.

(22) Oh, H.; Kim, H.; Yoo, H.; Park, B.; Chung, S.; Lee, B.; Hong, Y. Inkjet-printing-based density profile engineering of single-walled carbon nanotube networks for conformable high-on/off-performance thin-film transistors. *ACS Appl. Mater. Interfaces* **2021**, *13* (36), 43163−43173.

(23) Park, B.; Jang, J.; Kim, H.; Seo, J.; Yoo, H.; Kim, T.; Hong, Y. Enhanced current path by circularly and periodically-aligned semi-conducting single-walled carbon nanotubes for logic circuit device. *Flex. Print. Electron.* **2022**, *7* (1), 015005.

(24) Hu, L.; Hecht, D.; Grüner, G. Percolation in transparent and conducting carbon nanotube networks. *Nano Lett.* **2004**, *4* (12), 2513−2517.

(25) Qian, L.; Xie, Y.; Zhang, S.; Zhang, J. Band engineering of carbon nanotubes for device applications. *Matter* **2020**, *3* (3), 664−695.

(26) Saito, R.; Grüneis, A.; Samsonidze, G. G.; Brar, V.; Dresselhaus, G.; Dresselhaus, M.; Jorio, A.; Cançado, L.; Fantini, C.; Pimenta, M. Double resonance Raman spectroscopy of single-wall carbon nanotubes. *New J. Phys.* **2003**, *5* (1), 157.

(27) Dresselhaus, M.; Dresselhaus, G.; Jorio, A.; Souza Filho, A.; Pimenta, M.; Saito, R. Single nanotube Raman spectroscopy. *Acc. Chem. Res.* **2002**, *35* (12), 1070−1078.

(28) Popov, V. N.; Lambin, P. Radius and chirality dependence of the radial breathing mode and the G-band phonon modes of single-walled carbon nanotubes. *Phys. Rev. B* **2006**, *73* (8), 085407.

(29) Song, D.; Zare Bidoky, F.; Hyun, W. J.; Walker, S. B.; Lewis, J. A.; Frisbie, C. D. All-printed, self-aligned carbon nanotube thin-film transistors on imprinted plastic substrates. *ACS Appl. Mater. Interfaces* **2018**, *10* (18), 15926−15932.

(30) Li, Q.; Li, S.; Yang, D.; Su, W.; Wang, Y.; Zhou, W.; Liu, H.; Xie, S. Designing hybrid gate dielectric for fully printing high-performance carbon nanotube thin film transistors. *Nanotechnology* **2017**, *28* (43), 435203.

(31) Gao, W.; Xu, W.; Ye, J.; Liu, T.; Wang, J.; Tan, H.; Lin, Y.; Tange, M.; Sun, D.; Wu, L. Selective Dispersion of Large-Diameter Semiconducting Carbon Nanotubes by Functionalized Conjugated Dendritic Oligothiophenes for Use in Printed Thin Film Transistors. *Adv. Funct. Mater.* **2017**, *27* (44), 1703938.

(32) Cao, X.; Wu, F.; Lau, C.; Liu, Y.; Liu, Q.; Zhou, C. Top-contact self-aligned printing for high-performance carbon nanotube thin-film transistors with sub-micron channel length. *ACS Nano* **2017**, *11* (2), 2008−2014.

(33) Grubb, P. M.; Subbaraman, H.; Park, S.; Akinwande, D.; Chen, R. T. Inkjet printing of high performance transistors with micron order chemically set gaps. *Sci. Rep.* **2017**, *7* (1), 1−8.

(34) Cardenas, J. A.; Catenacci, M. J.; Andrews, J. B.; Williams, N. X.; Wiley, B. J.; Franklin, A. D. In-place printing of carbon nanotube transistors at low temperature. *ACS Appl. Nano Mater.* **2018**, *1* (4), 1863−1869.

(35) Lu, S.; Cardenas, J. A.; Worsley, R.; Williams, N. X.; Andrews, J. B.; Casiraghi, C.; Franklin, A. D. Flexible, print-in-place 1D−2D thin-film transistors using aerosol jet printing. *ACS Nano* **2019**, *13* (10), 11263−11272.

(36) Molina-Lopez, F.; Gao, T.; Kraft, U.; Zhu, C.; Öhlund, T.; Pfattner, R.; Feig, V.; Kim, Y.; Wang, S.; Yun, Y. Inkjet-printed stretchable and low voltage synaptic transistor array. *Nat. Commun.* **2019**, *10* (1), 1−10.

(37) Robin, M.; Portilla, L.; Wei, M.; Gao, T.; Zhao, J.; Shao, S.; Pecunia, V.; Cui, Z. Overcoming electrochemical instabilities of printed silver electrodes in all-printed ion gel gated carbon nanotube thin-film transistors. *ACS Appl. Mater. Interfaces* **2019**, *11* (44), 41531−41543.

https://doi.org/10.1021/acsaelm.2c01685
ACS Appl. Electron. Mater. 2023, 5, 2055−2064

(38) Chen, J.; Mishra, S.; Vaca, D.; Kumar, N.; Yeo, W.-H.; Sitaraman, S.; Kumar, S. Thin dielectric-layer-enabled low-voltage operation of fully printed flexible carbon nanotube thin-film transistors. *Nanotechnology* **2020**, *31* (23), 235301.
(39) Wang, X.; Wei, M.; Li, X.; Shao, S.; Ren, Y.; Xu, W.; Li, M.; Liu, W.; Liu, X.; Zhao, J. Large-area flexible printed thin-film transistors with semiconducting single-walled carbon nanotubes for NO2 sensors. *ACS Appl. Mater. Interfaces* **2020**, *12* (46), 51797−51807.
(40) Wei, M.; Robin, M.; Portilla, L.; Ren, Y.; Shao, S.; Bai, L.; Cao, Y.; Pecunia, V.; Cui, Z.; Zhao, J. Air-stable N-type printed carbon nanotube thin film transistors for CMOS logic circuits. *Carbon* **2020**, *163*, 145−153.
(41) Li, M.; Deng, J.; Wang, X.; Shao, S.; Li, X.; Gu, W.; Wang, H.; Zhao, J. Flexible printed single-walled carbon nanotubes olfactory synaptic transistors with crosslinked poly (4-vinylphenol) as dielectrics. *Flex. Print. Electron.* **2021**, *6* (3), 034001.
(42) Ren, Y.; Li, M.; Li, X.; Geng, Y.; Wang, X.; Zhao, J. High-performance flexible fully-printed all-carbon thin film transistors and ultrasensitive NH 3 sensors. *J. Mater. Chem. C* **2021**, *9* (6), 2133−2144.
(43) Lamberti, P.; Mousavi, S. A.; Spinelli, G.; Tucci, V.; Wagner, V. Fabrication and charge transport modeling of thin-film transistor based on carbon nanotubes network. *IEEE Trans. Nanotechnol.* **2014**, *13* (4), 795−804.
(44) Fujii, S.; Tanaka, T.; Miyata, Y.; Suga, H.; Naitoh, Y.; Minari, T.; Miyadera, T.; Tsukagoshi, K.; Kataura, H. Performance enhancement of thin-film transistors by using high-purity semiconducting single-wall carbon nanotubes. *Appl. Phys. Express* **2009**, *2* (7), 071601.
(45) Kim, J.; Hong, D.; Lee, H.; Shin, Y.; Park, S.; Khang, Y.; Lee, M.; Hong, S. Large scale assembly of pristine semiconducting carbon nanotube network-based devices exhibiting intrinsic characteristics. *J. Phys. Chem. C* **2013**, *117* (38), 19721−19728.
(46) Wang, C.; Zhang, J.; Ryu, K.; Badmaev, A.; De Arco, L. G.; Zhou, C. Wafer-scale fabrication of separated carbon nanotube thin-film transistors for display applications. *Nano Lett.* **2009**, *9* (12), 4285−4291.
(47) Ono, Y.; Kishimoto, S.; Ohno, Y.; Mizutani, T. Thin film transistors using PECVD-grown carbon nanotubes.*Nanotechnology***2010**, *21*, 205202.
(48) Park, B.; Jang, J.; Kim, H.; Seo, J.; Yoo, H.; Kim, T.; Hong, Y. Dense assembly of finely patterned semiconducting single-walled carbon nanotubes via a selective transfer method of nanotube-attracting layers. *ACS Appl. Mater. Interfaces* **2020**, *12* (34), 38441−38450.
(49) Seo, J.; Ha, J.; Lee, B.; Kim, H.; Hong, Y. Fluoroelastomer encapsulation for enhanced reliability of solution-processed carbon nanotube thin-film transistors. *Thin Solid Films* **2020**, *704*, 138021.
(50) Gao, T.; Deng, J.; Li, X.; Ren, Y.; Gu, W.; Robin, M.; Zhao, J. Printed solid state electrolyte carbon nanotube thin film transistors for sub-1 V fully printed flexible CMOS inverters. *J. Mater. Chem. C* **2021**, *9* (21), 6852−6862.
(51) Portilla, L.; Zhao, J.; Zhao, J.; Occhipinti, L. G.; Pecunia, V. Ambipolar carbon nanotube transistors with hybrid nanodielectric for low-voltage CMOS-like electronics. *Nano Futures* **2021**, *5* (2), 025001.
(52) Cardenas, J. A.; Lu, S.; Williams, N. X.; Doherty, J. L.; Franklin, A. D. In-place printing of flexible electrolyte-gated carbon nanotube transistors with enhanced stability. *IEEE Electron Device Lett.* **2021**, *42* (3), 367−370.
(53) Yanagi, K.; Udoguchi, H.; Sagitani, S.; Oshima, Y.; Takenobu, T.; Kataura, H.; Ishida, T.; Matsuda, K.; Maniwa, Y. Transport mechanisms in metallic and semiconducting single-wall carbon nanotube networks. *ACS Nano* **2010**, *4* (7), 4027−4032.
(54) Svensson, J.; Campbell, E. E. Schottky barriers in carbon nanotube-metal contacts. *J. Appl. Phys.* **2011**, *110* (11), 16.
(55) Lim, S. C.; Jang, J. H.; Bae, D. J.; Han, G. H.; Lee, S.; Yeo, I.-S.; Lee, Y. H. Contact resistance between metal and carbon nanotube interconnects: Effect of work function and wettability. *Appl. Phys. Lett.* **2009**, *95* (26), 264103.
(56) Kim, K. K.; Bae, J. J.; Park, H. K.; Kim, S. M.; Geng, H.-Z.; Park, K. A.; Shin, H.-J.; Yoon, S.-M.; Benayad, A.; Choi, J.-Y. Fermi level engineering of single-walled carbon nanotubes by AuCl3 doping. *J. Am. Chem. Soc.* **2008**, *130* (38), 12757−12761.
(57) Sarker, B. K.; Kang, N.; Khondaker, S. I. High performance semiconducting enriched carbon nanotube thin film transistors using metallic carbon nanotubes as electrodes. *Nanoscale* **2014**, *6* (9), 4896−4902.
(58) Chang, H.-Y.; Zhu, W.; Akinwande, D. On the mobility and contact resistance evaluation for transistors based on MoS2 or two-dimensional semiconducting atomic crystals. *Appl. Phys. Lett.* **2014**, *104* (11), 113504.
(59) Seong, N.; Kim, T.; Kim, H.; Ha, T.-J.; Hong, Y. Tunable threshold voltage in solution-processed single-walled carbon nanotube thin-film transistors. *Curr. Appl. Phys.* **2015**, *15*, S8−S11.

https://doi.org/10.1021/acsaelm.2c01685
ACS Appl. Electron. Mater. 2023, 5, 2055−2064